18TH WORLD CONFERENCE ON EARTHQUAKE ENGINEERING
WCEE2024
MILAN

MILAN, ITALY
30TH JUNE - 5TH JULY 2024

www.wcee2024.it

ADVANCES IN THE DESIGN OF ENERGY DISSIPATING DEVICES. EXPERIMENTAL AND NUMERICAL CHARACTERIZATION

J. Ramirez [1 2], G. Bozzo [2 3], F. Rastellini [1 2], J.M. Gonzalez [1 2], D. La Torre [4], A. Almeida [4], E. Valcarcel [4]

[1] Centre Internacional en Metodes Numerics a l'Enginyeria, Barcelona, Spain

[2] Universitat Politècnica de Catalunya (UPC), Barcelona, Spain

[3] SLB Devices, Barcelona, Spain

[4] Universidad de Lima, Lima, Peru

Abstract: *This study presents a numerical constitutive characterization of the behavior of a type of energy-dissipating device, known as Shear Link Bozzo (SLB). The SLBs are predominantly shear-based energy dissipation devices that feature a unique comb-type upper connection. This connection transmits the load to the working plate of the device without transmitting any axial force, allowing the plate to rotate in its plane. A set of experimental tests have been performed for geometries and typologies of the energy dissipation system. These tests follow a standard procedure based on cyclic and monotonic loads in order to characterize each device and determine its mechanical properties. The experiments were carried out in the structures laboratory of the University of Lima, Peru. Tridimensional numerical models are defined including the comb-type connection in order to characterize the devices tested for numerical simulation. The numerical models simulate the entire experimental test, including the loading protocols and the appropriate boundary conditions. Both the working plate and the comb-type connection have been modeled numerically and discretized with hexahedral solid elements and regular prisms. Mesh convergence studies are performed to evaluate the accuracy of the solution. An elastoplastic constitutive model with static and kinematic hardening parameters is employed to capture the mechanical behavior of the device. The numerical and experimental comparison is analyzed showing excellent correlation factors for the results obtained, like displacement, forces, dissipated energy, and effective stiffness. The optimal constitutive parameters for the correlation are presented. The numerical characterization here presented provides a powerful computational tool for the structural analysis of buildings and bridges under seismic conditions using the SLB dissipative dissipators.*

1. Introduction

SLB seismic energy dissipators are devices that operate through metal yielding and thanks to their substantial stiffness, they enable the creation of structures that are both rigid and ductile, capable of withstanding severe seismic events with minimal structural damage.

SLB dissipators emerged in the early 2000s as energy dissipators designed primarily for masonry walls. Their design is based on the same operational principle as the dissipative structural system for eccentrically braced frames developed by Popov and Engelhardt (Popov et al., 1987). Because steel is a material that performs very well dissipating energy, especially under shear forces, the application of these dissipators was extended beyond masonry walls to encompass structures made of both steel and concrete. This research led to the second generation of devices that reached deformations of up to 3 cm. Both the first and second generations of devices featured bolted connections at both ends, resulting in a fully restrained condition within the device (fixed in both ends). To enhance the applicability of this system a gear or “toothed” connection was introduced, abandoning the previous double fixed connection into a fixed-articulated boundary condition. These devices were named as the third generation.

Both the second and third generations, although different boundary conditions, had the same deformation capacity. It wasn't until the research led by G. Bozzo in 2021 that a fourth generation emerged. This new generation allowed reaching deformations of up to 5 cm in the devices while still maintaining the gear

connection (Bozzo, 2021). In order to validate the research, experimental testing of this generation was carried out in laboratories of the University of Cantabria (LADICIM), Spain, following the loading protocols of AISC 341-16 (AISC, 2016; LADICIM, 2020).

Figure 1. Shear Link Bozzo Devices

The use of seismic protection systems in structural design has gained popularity since the 1980s (Bozzo and Barbat, 1999). Moving away from conventional seismic design based on structural redundancy, seismic protection allows for more optimal material density in structure design, better earthquake response, and easier post-earthquake inspection and repair if needed. Among seismic protection systems, we can highlight base isolation and energy dissipators as two very popular alternatives. Base isolation is highly effective only in medium to low-rise buildings as it decouples the superstructure from the ground and therefore has to support it so high-rise buildings are not adequate. This system allows for significantly reduce earthquake-induced forces, however, it entails significant costs, complexity, and design challenges, especially because the entire superstructure relies on it, and any failure or obstruction of the system could lead to the collapse of the entire structure.

To date, SLB dissipators have been tested in over six countries, including Italy, Portugal, Spain, and Peru. For the study presented in this paper, tests conducted at the University of Lima's laboratory in Peru have been used. This laboratory is equipped with cutting-edge technology, including a brand new +/-1000kN hydraulic press machine or a 6-meter tall reaction wall. Since 2022 this laboratory has conducted more than 20 tests on various SLB specimens achieving displacements of over 8cm and 700kN. Energy dissipators provide a compelling alternative for medium to high-rise buildings. In particular, SLB dissipators offer a wide range of applications due to their mechanical properties, mostly due to their high stiffness and their lack of axial load transmission. To date, they have been employed primarily in both new and retrofit building projects, although there are also studies validating their use in wind towers and high-rise bridges (Illarregui, 2021). Among the projects featuring SLB dissipators, there are towers exceeding 200 meters in height and 60 stories, such as the Paradox Tower and the Oak 58 Tower, both located in Mexico.

These devices are commonly made of steel, an isotropic material that is easily characterized. However, due to the geometric complexity and the large deformations required in these devices, precise numerical modeling of the entire system is highly complex. Additionally, the high stiffness of these devices makes experimental testing challenging since it requires an even more rigid supporting auxiliary structure for stable testing under proper boundary conditions, along with a hydraulic press machine capable of applying the high forces required for testing. SLB devices are steel-made dissipators, constructed from an isotropic material that is easy to characterize. Uncertainty in their characterization mainly arises from geometry, accentuating such uncertainty for large deformations since second-order effects come into play. Numerical characterization helps reduce the uncertainty of the devices, aiding in the selection of the best prototypes to be tested and predicting their behavior.

2. Experimental Testing

The tests were carried out in the laboratory of the University of Lima, Peru. To conduct them, a hydraulic press with the capacity to apply loads of +/- 1000kN (compression/tension) was used. The devices were tested using an auxiliary structure that allowed them to be set up as cantilevers to simulate the proper application of load on the devices, which operate solely under shear. Additionally, in order to capture all displacements during the tests, Linear Variable Differential Transducers (LVDTs) were employed. These devices enable the measurement of all motions from both the device and the auxiliary structure. LVDTs are a common type of electromechanical transducer that can convert the motion of an object into a corresponding electrical signal (Bozzo et al., 2023).

Figure 2 illustrates the LVDT configuration employed for the testing. Five transducers were used, three for monitoring the displacements of the tested device, with two of them dedicated to its vertical movement and one for horizontal (out of plane) motion, and two LVDTs for tracking the motions of the auxiliary structure, ensuring its stability under the compression or tension loads applied to the devices. This configuration ensured verifying the boundary conditions as well as the device response to the load.

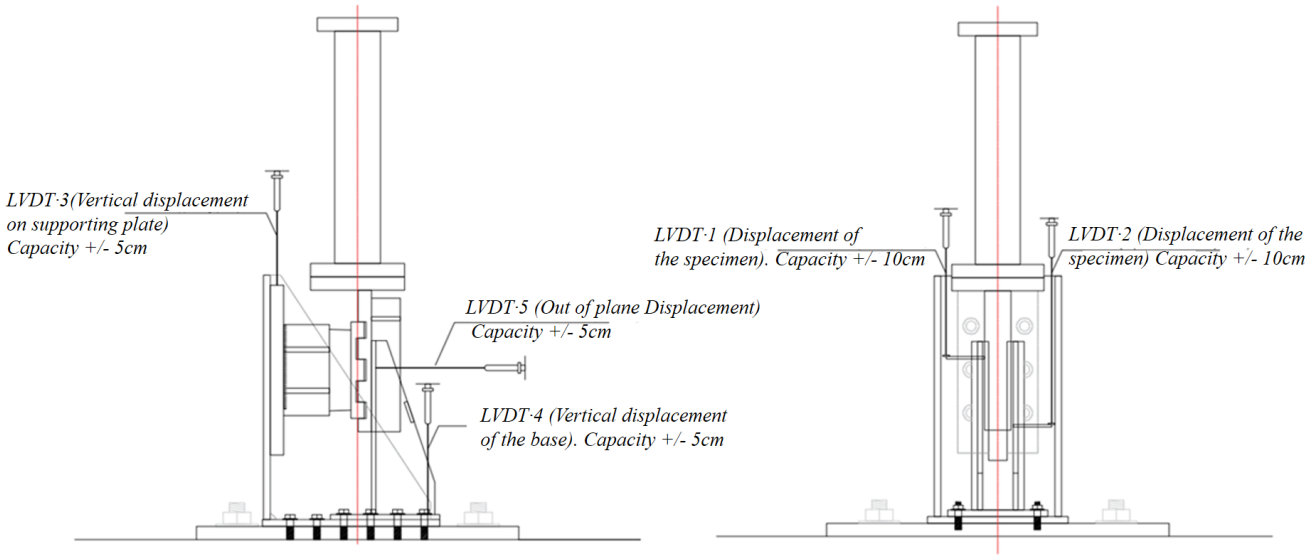

Figure 2. Lateral and Frontal View of LVDT Configuration

The tests were conducted following the loading patterns recommended by the AISC 360-16 code (AISC, 2016). This loading pattern is defined by the application of complete cyclic loads on the device, reaching up to 32mm of displacement. Figure 3 displays the results obtained through the instrumentation. It presents the hysteresis curves captured by LVDT 1, illustrating how they reach up to 32mm of displacement. It also shows the displacement recorded by the other LVDTs with a maximum displacement of 0.5mm. Thereby confirming the adequate elastic response of the auxiliary structure and validating the data acquired.

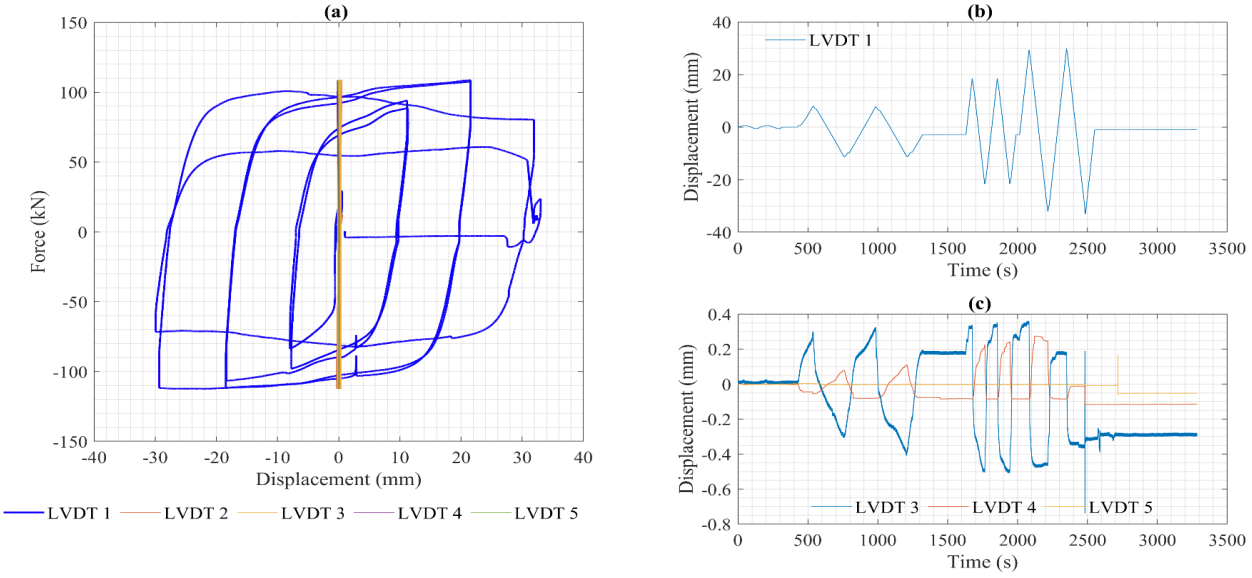

Figure 3. Experimental results

3. Numerical Modeling

FEM numerical models have been initially developed using the code COMPACK. The International Center for Numerical Methods in Engineering (CIMNE) has internally developed this program, and it operates within the framework of simulating dynamic analyses of composite structures using the incremental explicit approach and employing the theory of the finite element method, as discussed by *Rastellini et al. (2008), Martinez et al. (2008), and Rastellini et al. (2016).*

3.1. FEM model

The SLB energy dissipation system comprises the device and its unique comb connection, illustrated in Figures 4a, and 4b. The results obtained in these tests are precisely reproduced by numerical models in the cyclic loading tests. For this research, the third-generation dissipator SLB2 10_3 has been selected as the central focus of the numerical simulation.

The SLB dissipative components showcase distinctive, variable, waist-shaped, and symmetrical geometries, distinguishing them from conventional designs, see Figure 4c. These components are made of a rigid frame adjusted to specific design parameters and highlight dissipative windows with rounded edges, machined to a reduced thickness automatically. Using a regular discretization approach, a combination of hexahedral solids and regular triangular-based prisms is employed. Isoparametric 8-node 3D hexahedral solids are used with a Gaussian point integration scheme for shear and uniform volumetric deformation. The Total Lagrangian formulation is used to describe geometric non-linearities, assuming an additive decomposition of the logarithmic strain tensor for large non-elastic deformations, (*Flores, 2001).*

The special connection positioned at the top of the dissipators comprises two rigid metallic components separated by a distance of 0.5 mm. These components come into contact with cyclic loads and are arranged to prevent the transmission of axial loads. In the model, it is defined as an undeformable element modeled by a structured mesh of regular triangles, as shown in Figure 4d.

The connection components offer a sophisticated design capable of managing cyclic loads and geometric non-linearities. The combination of specific geometries with a regular discretization approach adds robustness to the design, enabling it to address significant deformations without compromising the effectiveness of the components. The specific arrangement of the connection, along with the ability to prevent the transmission of axial loads, demonstrates meticulous consideration to maximize the efficiency and durability of the system in dynamic loading environments, see Figure 4d.

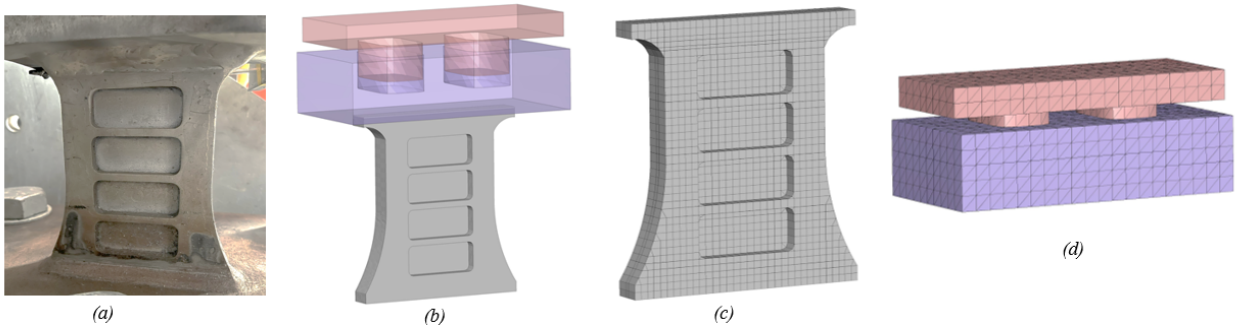

Figure 4. a. Geometry of SLB 2 10-3. b. FEM Modeling of the SLB system. c. SLB Devices Discretization. d. Comb-Type Special Connection Discretization.

3.2. Nonlinear Behavior in Modeling

The development of the FEM model for a dissipator entails inherent complexity due to the presence of two types of nonlinearities. Firstly, the dissipator material nonlinearity requires experimental calibration to accurately characterize the material, typically ASTM A36 steel. This calibration involves defining a combined, isotropic, and kinematic hardening model essential for capturing the material's response to cyclic loads during seismic events. Additionally, the second nonlinearity, associated with contact in the comb-type connection, is addressed through a specific algorithm based on the penalty method. These approaches aim

to ensure the accuracy and reliability of the model in representing the dissipator's behavior under seismic conditions. These considerations will be detailed in the following sections.

3.2.1.Material Constitutive Model

The SLB seismic protection system operates by inducing plastic deformation with stress dissipation until dents form in the metallic component. ASTM A36 structural steel is the material used in these devices. To evaluate nonlinear behavior accurately, conducting an experimental calibration is crucial. This calibration involves establishing a combined hardening model, incorporating both isotropic and kinematic components, to depict how the material responds to cyclic loads experienced during seismic events.

In recent years, computational mechanics has seen notable advancements, with the Yoshida-Uemori (Y-U) isotropic and kinematic hardening plasticity model standing out. This model is specifically designed to describe the response of metals to cyclic loads, including mild steels, high-strength steels, and aluminum alloy sheets, particularly under conditions of significant deformation *(Yoshida and Uemori, 2002; Yoshida and Uemori, 2003).*

The constitutive model exhibits a high capability to depict both high deformation cyclic plasticity and stress-strain responses at a small scale following substantial pre-deformation. Furthermore, it excels at accurately predicting the mechanical response of metallic materials subjected to cyclic loads, displaying anisotropic behavior.

Compared to other constitutive theories, the Yoshida-Uemori approach is considered the most consistent, capable of accurately simulating the transient Bauschinger effect, permanent softening, and strain hardening stagnation under large elastoplastic deformations *(Fincato et al., 2021)*. This model, surpassing the limitations of traditional approaches, stands out for its precision, particularly in characterizing kinematic hardening. This ability effectively captures the complex behavior of energy dissipators. It is valuable in characterizing special metals and alloys, making it a significant choice for simulating SLB energy dissipators due to its capacity to represent significant plastic deformations in response to seismic excitations.

Within Compack, fundamental mechanical properties of elastic materials are defined by parameters such as Young's Modulus (*Eo)*, Poisson's Ratio (*μ)*, and the material density (*ρ)*. Additionally, the elastic parameters within the Yoshida Uemori formulation are introduced, notably the prestrain-dependent Young's modulus (*Ea)* and the exponent (*ξ)* governing the Young's Modulus change. On another front, pivotal plasticity parameters come into play, including Yield Strength (*Y)*, the experimental adjustment parameter (*b)*, the parameter (*C)* defining the kinematic hardening rate on the yield surface, (*m)* governing the isotropic and kinematic hardening rate at the yield limit, the initial yield surface radius (*B)*, the saturation limit stress for infinitely large strains (*Rsat)*, and the parameter (*h)* regulating the expansion rate of the yield surface. An adjustment will be made using these parameters to accurately calibrate both the numerical model according to the experiment, as seen in item 4.

3.2.2. Contact nonlinearity

Mechanical contact, particularly evident in the comb connection parts introduces significant nonlinearity under cyclic loading. Figure 5 shows the configuration of the contact between the lower and upper connection, displaying the contact interface surfaces.The Compack program is specifically designed to analyze contact issues in sheet stamping processes, handling considerable deformations regardless of the presence of friction.

Utilizing an advanced three-dimensional contact algorithm, the program incorporates the penalization method explained by *Agelet de Saracibar (1990), Zhong (1993), and Flores (2000)*. It also considers friction using Coulomb's law. This method is widely used and compatible with explicit integration models, enabling the interpolation of contact surfaces using triangular or quadrilateral segments.

In this methodology, no friction between the upper and lower components is no considered. The software checks for the penetration of each slave node into the master surface. Upon detecting penetration, it calculates and applies an interface force between the slave node and the corresponding master nodes. The force is determined by the depth of penetration and a penalization coefficient.

To ensure a symmetrical treatment at the contact interface, the program verifies the potential penetration of the master nodes through the slave surface. Its contact search procedure primarily focuses on identifying nodes in contact and potential segments by locating the nearest master node for each slave node. The surrounding segments are carefully examined for any signs of penetration.

3.3. Boundary and Kinematic Conditions

Finite Element Models incorporate customized boundary conditions for accurately showing how the system reacts under specific test parameters. By using the 'master-slave' condition, the non-deformability of the connections is ensured, with nodes fixed to defined nodes. Both the lower connection and the upper part of the dissipator are fixed using 'master-slave.' Additionally, the experimental displacement curve is assigned to the upper connection of the SLB system.

At first, a fixed base was contemplated for the dissipator. However, upon recognizing the flexibility of the system, the decision was made to incorporate hexahedral elastic solids underneath the dissipative components, as shown in Figure 6. By including these hexahedral solids, the intention was to enhance the overall system flexibility and its response to cyclic loads. Additionally, this addition aimed to reduce the stiffness slope of the SLB system in a hysteresis curve, providing a clearer illustration upon closer examination.

These procedures and assumptions define the methodology employed, portraying damping characteristics similar to those observed in a quasi-static analysis. The FEM models incorporate boundary conditions adjusted to align with the conducted tests. To achieve a precise correspondence with real-world behavior, the experimental displacement curve (LDVT 1) is assigned to the representation of the upper connection of the SLB system. Additionally, a "master-slave" condition is employed based on nodal dependence within the inferior connection to enhance its stiffness.

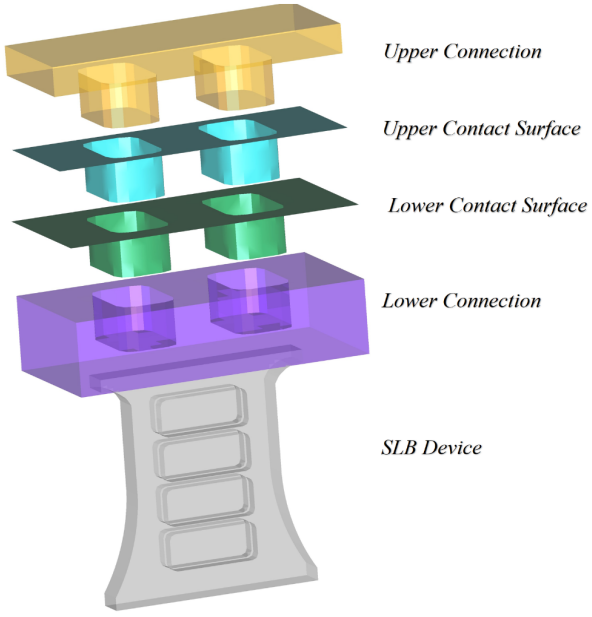

Figure 5. Mechanical contact surfaces in the SLB system

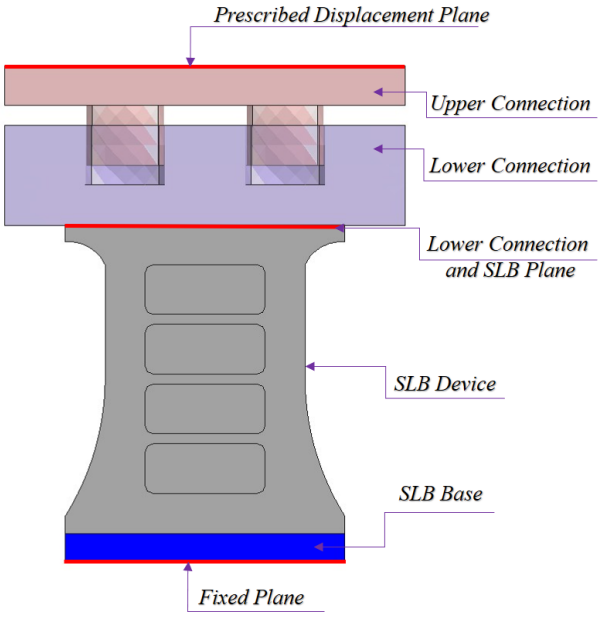

Figure 6. Boundary and Kinematic Conditions in FEM Modeling

4. Experimental-Model Numerical Characterization

The characterization of the structural response of the dissipator is performed using the numerical model to reproduce the experimental test, through the calibration of the constitutive parameters and the adjustment of the boundary conditions and contact algorithm. This section shows this process, the results obtained and its validation. Key information about the properties of the seismic dissipation devices used in the model enhances our analytical framework. The ASTM A36 steel has a density of ρ=7800 kg/m³, an elastic modulus

of Eo=206GPa, and a Poisson's ratio μ=0.30. The discussion starts by outlining the material parameters according to the Yoshida-Uemori model, describing the specific properties employed in the numerical simulations detailed in Section 3.2.1 and presented in Table 1.

Plasticity parameters							**Parameters for prestrain dependent Young's moduli**		
Y [MPa]	***b*** [MPa	**C**	**m**	***B*** [MPa]	**Rsat** [MPa]	**h**	**Eo** [GPa]	**Ea** [GPa]	**ξ**
143	23	557	29	280	147	0.50	206	160	60

Table 1. Material parameters in Yoshida - Uemori model

The experimental numerical correlation section will address the comparison between numerical and experimental data, focusing on various aspects such as hysteresis curves, energy dissipation capacity, stiffness degradation, effective stiffness, and the equivalent viscous damping coefficient.

4.1 Hysteretic curves

This section examines the correlation between numerical and experimental data, particularly scrutinizing the temporal evolution of forces and displacements in a significant hysteresis curve for our study. Figure 7 illustrates the hysteresis curves from the experimental test and the Finite Element Method (FEM) model with a dissipator on a rigid base, whose material is defined by the parameters of the Yoshida Uemori model (Table 1). Point A, representing the experimental curve data, stands out, showcasing the dissipator's failure mode. To adequately characterize and compare the results, we analyze the curves obtained up to point A.

According to Figure 3c, the displacements recorded by the LVDT show variations in the testing machine. Consequently, a flexible base is included in the model to provide flexibility to the system, as specified in section 3.3. Figure 8 displays the hysteresis curves of both fixed and flexible base cases, along with the experimental results. This figure illustrates the variations in the stiffness of the solids that make up the support base of the SLB system, which justifies the addition of the flexible base.

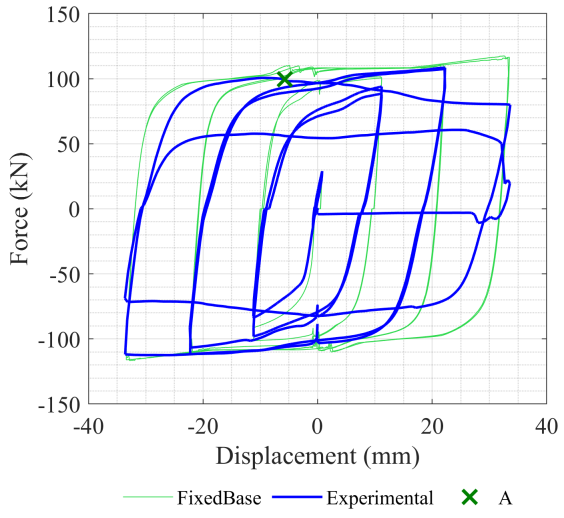

Figure 7. Hysteretic curves. Fixed base dissipator and experimental result

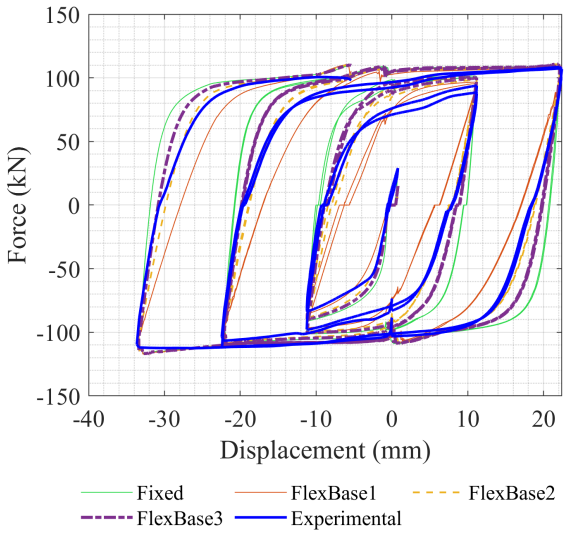

Figure 8. Hysteresis Curves. Fixed, flexible base cases and experimental result

To assess the sensitivity and the effect of mesh discretization in FEM models of the SLB system, three types of meshes were generated for the devices and their elastic base using finite elements, as shown in Figure 9. These meshes for the dampers are defined as 'mesh1' with 5372 hexahedra, 'mesh2' with 6146 hexahedra, and 'mesh3' with 23862 hexahedra. Regarding execution time, on a 16-core computer, the coarse mesh case takes 2 hours and 17 minutes, the medium mesh approximately 14 hours and 56 minutes, and an estimated 29 hours for the finest mesh.

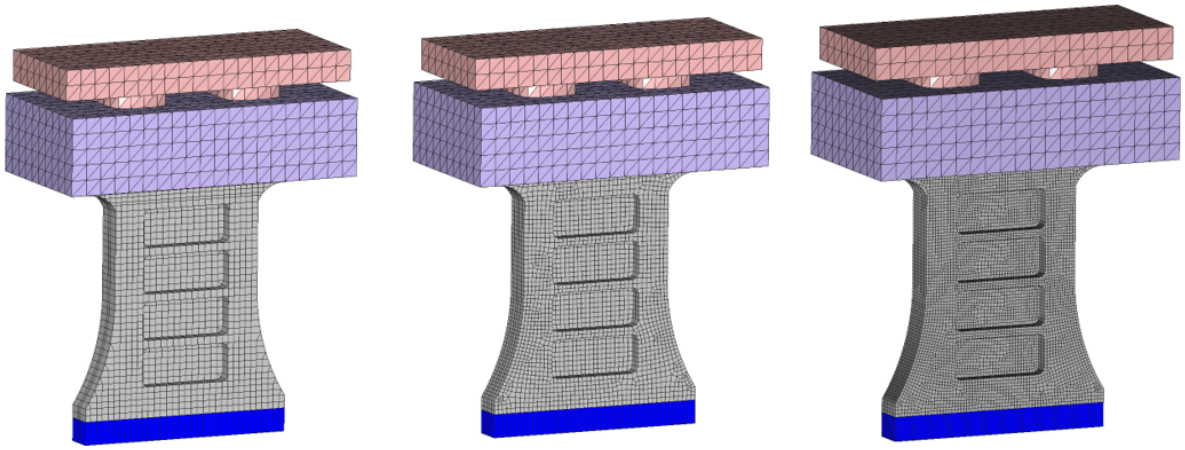

Figure 9. Meshes SLB system: Mesh1, Mesh2, and Mesh3

4.2. Energy dissipation capacity

The energy absorbed by the SLB system can be measured as the space inside the hysteresis curve. In Figure 11, the accumulated energy obtained from both real tests and the FEM model is displayed. The total energy dissipated in each cycle increases as the displacement increases. Also, the accumulated energy keeps increasing as there are more displacements and deformations in the material. The accumulated energy is between 25 and 27 kN.m, slightly lower in the experimental test compared to the numerical simulation.

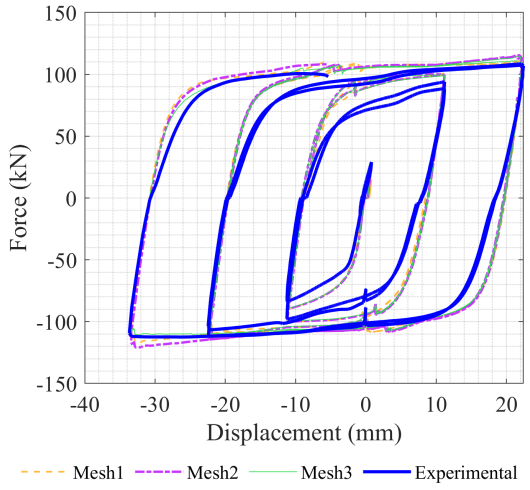

Figure 10. Hysteretic curves of meshes SLB system

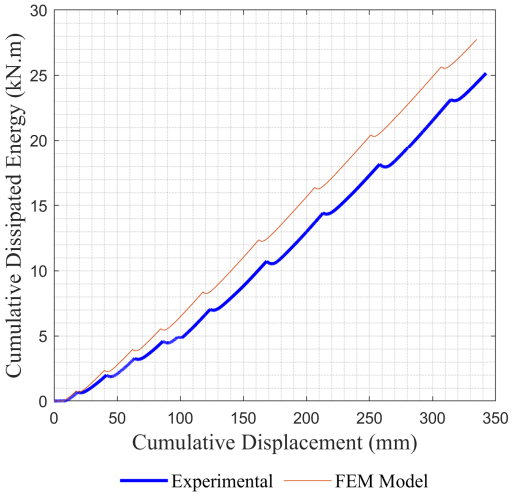

Figure 11. Cumulative Dissipated Energy

4.3. Stiffness Degradation and Effective Stiffness

Figure 12 shows the degradation of the Secant Stiffness of the experimental test and the calibrated FEM models. The degradation of secant stiffness is the relative appearance and development of cracks, the appearance of steel's plastic deformation that can represent the seismic capacity of the SLB device. The degradation of the Secant Stiffness can be estimated using the following expression:

$$K_i = \frac{|F_i|}{|X_i|} \quad (1)$$

where Fi denotes the load, while Xi represents the displacement at the i-th peak. (Ya Yang et al, 2023).

An analysis of structure responses with a linear dynamic analysis requires effective stiffness. Figure 13 illustrates the physical meaning of effective stiffness defined by the following equation (Teruna et al., 2015):

$$K_{eff} = \frac{|P^+| + |P^-|}{|\delta^+| + |\delta^-|} \quad (2)$$

where P denotes the force and δ represents the displacement in each cycle. Both figures show a good agreement between the experimental and the numerical curves obtained with the calibrated model.

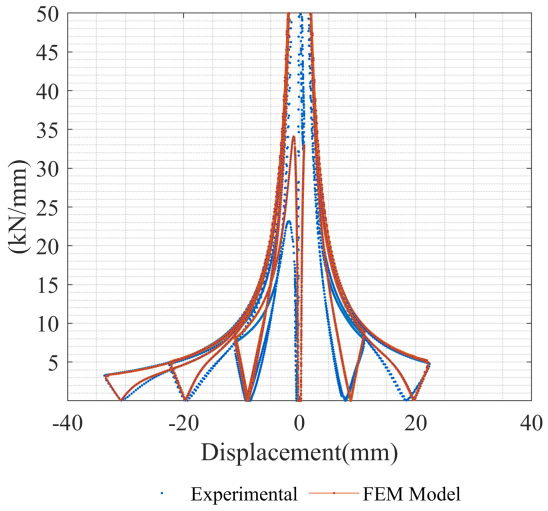

Figure 12. Stiffness degradation curve

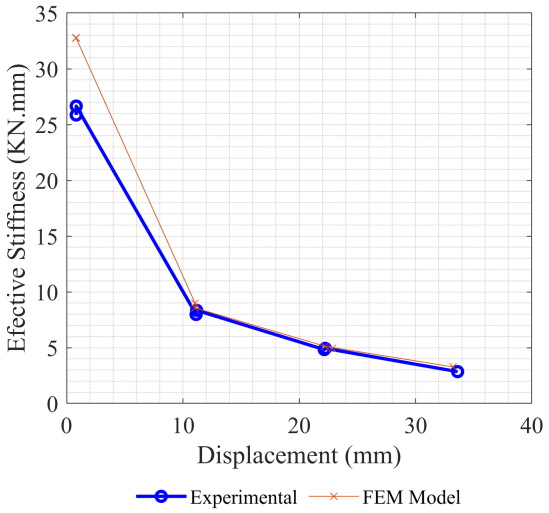

Figure 13. Effective stiffness

4.4. Equivalent Viscous Damping Coefficient

For damper devices, another important energy dissipation index is the equivalent damping ratio (Chopra, 1995), which is based on an equivalent viscous system as shown in Figure 14. The equivalent damping coefficient is defined as ξeq, which can be obtained by the following expression:

$$\xi_{eq} = \frac{1}{2\pi} \cdot \frac{E_d}{E_{sd}} = \frac{1}{2\pi} \cdot \frac{Area(FBE + FDO)}{Area(AOB + COD)} \quad (3)$$

Where Ed represents the measured energy dissipated by the hysteretic loops of devices, and Esd denotes the energy stored in an equivalent elastic spring.

The results for the equivalent viscous damping coefficient are depicted in Figure 15. It can be inferred that the equivalent viscous damping coefficient falls within the range of 0.48 to 0.54 for displacements between 22.2 and 33.2mm

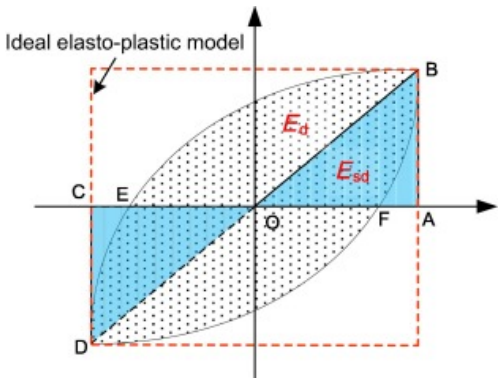

Figure 14. The energy dissipated and equivalent damping ratio in a cycle. Li-Yan Hu et al (2016)

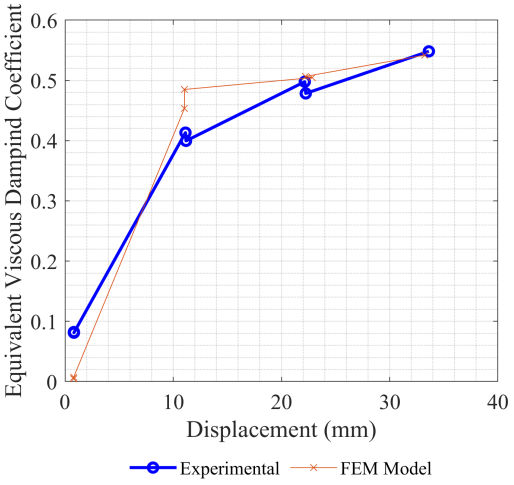

Figure 15. Equivalent Viscous Damping Coefficient

5. Analysis of results from the FEM model

This section displays some interesting results from the FEM model under load and unload test of the SLB seismic protection system.

To post-process the calculations carried out in COMPACK, the post-processor GiD Version v16.1.5.d is used. Figure 16 shows the plastic hardening values when applying a load-unload cycle in the simulated dissipator. It can be observed how the second upper window concentrates high plasticity index values, indicating a potential dent in that area and stress concentration. This latter observation is depicted in image 17, displaying the distribution of equivalent stresses at a specific moment of the simulation. Additionally, it is noticeable that there are no penetrations or failures in the defined contact zone.

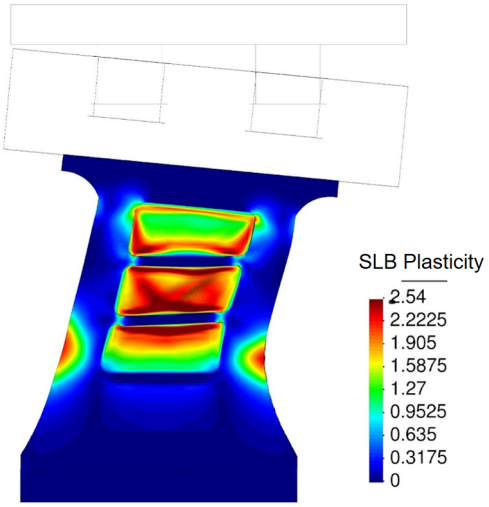

Figure 16. Plastic hardening in FEM Model

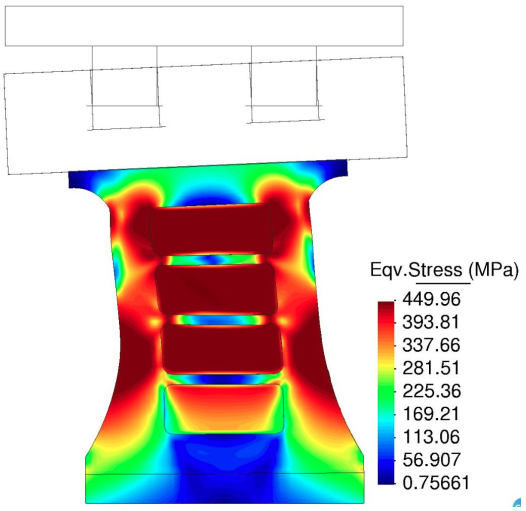

Figure 17. Equivalent Stress in FEM Model

Figure 18a presents a graphical comparison to the conducted test, while Figure 18b shows a post-process of the numerical model's deformation. It shows the failure mode or performance of the dissipative piece (local buckling and buckling). Figure 18c illustrates displacements along the Z-axis, perpendicular to the loading plane. Positive and negative displacements can be observed in the windows, indicating that the numerical simulations were consistent with the test results.

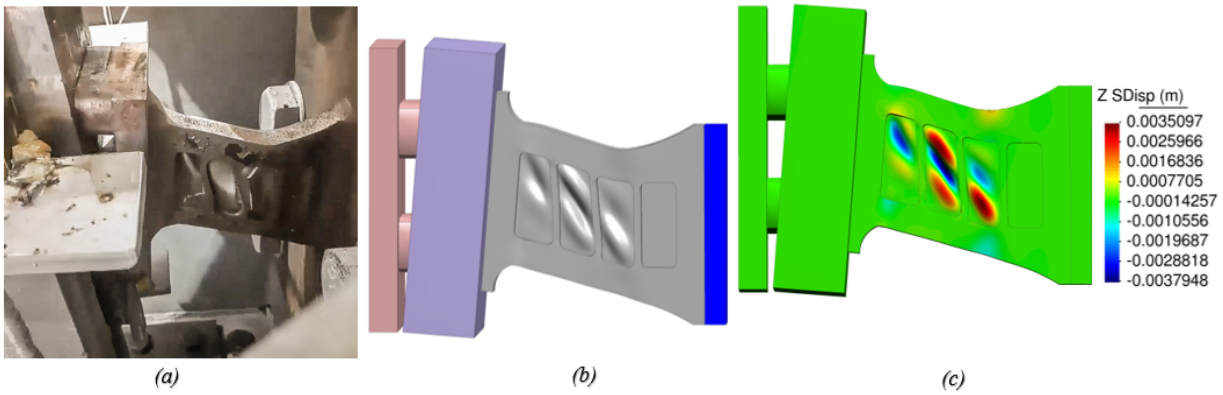

Figure 18. (a) SLB Cyclical Load Test. (b) Deformed FEM model. (c). z-displacements represent the failure mode of the dissipater.

5. Conclusions

Earthquake protection systems represent an efficient and practical solution in seismic-resistant design because they allow us to move away from the classical design based on structural redundancy in favor of a specialized system that absorbs deformations, thereby protecting other structural elements. Ongoing research in these systems enables us to achieve better knowledge of performance levels and expand their field of use. Thanks to this research we were able to achieve a very precise representation of the SLB device behavior under cyclic loading. This research led to a numerical-experimental methodology to characterize the structural response of a SLB device under seismic conditions. A numerical model based on the FEM is built including proper boundary conditions and contact surfaces, as long as a constitutive model and nonlinear formulations, to reproduce the dissipater response.

After the calibration of the constitutive parameters, the numerical results were validated against the experimental results, showing a good agreement in the hysteretic curves, but also in the specific parameters of the device like energy dissipation, effective stiffness, and viscous damping coefficients.

The numerical models ensure a comprehensive and accurate representation. considering the nonlinear behavior of materials in the simulations allows for a physical response. Incorporating precise mechanical contact parameters portrays the complex interactions of components in the structure. Finally, parameter calibration guarantees a close alignment with physical laboratory testing. The numerical model showed its capability to reproduce the buckling behavior observed in the device.

6. References

AISC. (2016). *Specification for Structural Steel Buildings*. Illinois.

Agelet de Saracibar, C. (1990). *Finite Element Analysis of Sheet Forming Processes*. Universitat Politécnica de Catalunya, Barcelona, Spain.

Bozzo, G. (2021). *Una nueva generación de disipadores SLB "Shear Link" para el diseño sismorresistente.* Universidad Politécnica de Cataluña.

Bozzo, L. M., & Barbat, A. H. (1999). *Diseño sismorresistente de edificios - Técnicas convencionales y avanzadas*. Barcelona: REVERTE.

Bozzo, G., Pérez, L., Miranda, E., Bairan, J., & Bozzo, L. (2023) *Optimal set-up configuration for testing stiff energy dissipating devices under large displacements*.

Chopra, A. K. (1995). *Dynamics of Structures*. Prentice Hall. Inc. USA, 729.C.

Fincato, R., Tsutsumi, S., Zilio, A., Mazzucco, G., & Salomoni, V. (2021). *Fully implicit numerical integration of the Yoshida-Uemori two-surface plasticity model with isotropic hardening stagnation.* Frattura ed Integrità Strutturale, 15(57), 114-126.

Flores, F. G. (2000). *Un algoritmo de contacto para el análisis explícito de procesos de embutición. Revista internacional de métodos numéricos.*

Flores, F. G. (2001). *Elementos finitos para el análisis de sólidos anisótropos con grandes deformaciones plásticas*. Mecánica Computacional, (5), 171-178.

Illarregui, N. (2021). *Disipación de energía sísmica en puentes de luces continuas.* Universidad Politécnica de Cataluña.

LADICIM (2020). *Caracterización mecánica de disipadores SLB (Informe Nº20208/01)*. Universidad de Cantabria, 16p.

Martinez, X., Oller, S., Rastellini, F., & Barbat, A. (2008). *A numerical procedure simulating RC structures reinforced with FRP using the serial/parallel mixing theory.* Computers and Structures, 86(15–16), 1604-1618.

Popov, E. P., Kasai, K., & Engelhardt, M. (1987). *Advances in design of eccentrically braced frames.* Bulletin of the New Zealand National Society for Earthquake Engineering.

Rastellini, F., Oller, S., Salomón, O., & Oñate, E. (2008). *Composite materials non-linear modelling for long fibre-reinforced laminates: Continuum basis, computational aspects and validations.* Computers & structures, 86(9), 879-896.

Rastellini, F., Socorro, G., Forgas, A., & Onate, E. (2016, August). *A triaxial failure diagram to predict the forming limit of 3D sheet metal parts subjected to multiaxial stresses*. Journal of Physics: Conference Series, 734(3), 032020.

Yang, Y., Gao, S., Zheng, Y., Liu, X., Zhang, W., & Lin, B. Q. (2023). S*eismic performance of precast column-beam joint with artificial plastic hinge.* Journal of Building Engineering, 67, 105942.

Yoshida, F., & Uemori, T. (2002). *A model of large-strain cyclic plasticity describing the Bauschinger effect and workhardening stagnation*. International journal of plasticity, 18(5-6), 661-686.

Yoshida, F., & Uemori, T. (2003). *A model of large-strain cyclic plasticity and its application to springback simulation.* International Journal of Mechanical Sciences, 45(10), 1687-1702.

Yoshida, F., Uemori, T., & Fujiwara, K. (2002). *Elastic–plastic behavior of steel sheets under in-plane cyclic tension–compression at large strain.* International journal of plasticity, 18(5-6), 633-659.

Zhong, Z. (1993). *Finite Element Procedures for Contact Impact Problems.* Oxford Univ. Press.